

PRECISION POSITION TRACKING OF MR-COMPATIBLE PNEUMATIC PISTON-CYLINDER USING SLIDING MODE CONTROL

David Comber

Department of Mechanical Engineering
Vanderbilt University
Nashville, TN 37235
david.b.comber@vanderbilt.edu

Eric J. Barth

Department of Mechanical Engineering
Vanderbilt University
Nashville, TN 37235
eric.j.barth@vanderbilt.edu

ABSTRACT

This paper presents the nonlinear dynamics and sliding mode control design for a 1-DOF needle insertion robot. The robot actuator is an MR-compatible pneumatic piston-cylinder. A brief review of the dynamics for this type of actuator is provided. The reaction force of tissue on the needle remains an unknown for which our controller compensates. A sliding mode control law is formulated that relies solely on position and pressure measurements (no force sensor). Experimental implementation of the actuator and controller is described. The mean and maximum steady-state position errors for step reference positions were 0.018 mm and 0.028 mm, respectively.

NOMENCLATURE

A_i Area of i th side of piston
 A_r Cross-sectional area of piston rod
 A_v Signed area of valve orifice
 β Piston-chamber wall viscous friction coefficient
 C_f Valve discharge coefficient
 C_r Critical pressure ratio
 e Position tracking error
 k Ratio of specific heats
 λ Repeated pole location of desired error dynamics
 \dot{m}_i Mass flow into i th chamber
 M Total mass of moving parts (piston, rod and needle)
 η Sliding mode robustness gain
 P_i Pressure of i th chamber

P_{atm} Atmospheric pressure
 P_s Supply pressure
 P_u Upstream pressure
 P_d Downstream pressure
 Ψ_i Area normalized mass flow
 R Specific ideal gas constant
 T Ambient temperature
 x Actuator position
 x_d Desired (reference) actuator position

INTRODUCTION

Precise needle tip placement is required for many surgical interventions, such as biopsy, thermal ablation, brachytherapy and deep brain stimulation. In these procedures, accurate positioning of the needle tip is limited by several factors, including tissue deformation, registration error and dependence on hand-eye coordination. Target accuracy has generally improved in recent years due to the development and use of image-guided surgical robots. Furthermore, real-time imaging during surgery can streamline procedures by reducing or eliminating the need for pre-operative imaging. For neurosurgical applications the need for intraoperative imaging is particularly great, since “brain shift” error typically occurs when only pre-operative imaging is available.

Because magnetic resonance imaging (MRI) generally provides the most informative type of medical images, there is substantial interest in developing fully MRI-compatible surgical robots. Indeed, many of these devices have been invented in the past fifteen years, and the extreme conditions of the MRI

operating environment have been surmounted by remarkable innovations.

Because MRI machines produce strong magnetic fields, fast-changing magnetic field gradients, and powerful radiofrequency pulses, conventional mechatronic systems are not suitable for MR-guidance applications. Any electromagnetic actuator found in such systems cannot be used because its ferrous core renders it not MR-safe. MR-compatible systems require alternative forms of actuation that both are non-magnetic (MR-safe) and do not malfunction due to the magnetic fields nor generate image artifacts (MR-compatible).

Four general types of actuation are used in MR-compatible robots: manual, hydraulic, ultrasonic motors and pneumatic. Manual actuation has been implemented successfully in devices for prostate brachytherapy. Namely, Krieger et al achieved better than 2mm accuracy with a 3-DOF manually actuated robot under 1.5T imaging; the authors later modified this system to employ ultrasonic motors [1],[2]. While manual actuation is fully MR-compatible, it is also the slowest type of system to operate and has not reduced procedure times to the same extent as other forms of MR-compatible actuators.

Kim et al and Moser et al have shown hydraulic actuators to be a viable technology in MR-compatible systems [3],[4]. However, Kim et al encountered problems with air bubbles in the fluid system and with fluid leakage. Similarly, Elhawary et al note that for hydraulic systems, there is the risk of contamination of the sterile environment in the event of a fluid spill, as well as a safety risk at the typical operating pressure of 15 bar [5].

Reviewing the spectrum of MR-compatible actuators, Tsekos et al conclude that the majority of robotic systems have used ultrasonic, piezoelectric motors (USM) [6]. While USM's provide many desirable characteristics, such as high torque, low backlash and a hard brake, commercially available USM's must be located far from the center of the magnet in order to realize acceptable signal-to-noise ratio (SNR). This restriction is inherent to the high frequency power supply for USM's. Furthermore, even with a substantial distance between magnet center and motor, the motors must power down during imaging. Krieger et al reported 40% to 60% reduction in SNR when USM's were enabled, which arguably precludes simultaneous imaging and actuation [2].

Elhawary et al review several MR-compatible systems employing USM's, all remotely actuated through mechanisms like drive shafts, belt or chain drives, and linkages [5]. These transmissions can result in undesirably large robots. For example, while Larson et al achieved sub-millimeter accuracy at 4T with a 5-DOF robot for stereotactic breast interventions, the authors note that larger patients cannot fit inside the scanner because the telescoping robot substantially reduces the clearance [7]. Wang et al successfully demonstrated a 6-DOF robot that can image under standard high field diagnostic

magnet (3T) with the USM's running and also located next to the head coil. However, preservation of a high SNR required substantial modifications to the USM drivers [8].

To a lesser extent than USM's, pneumatic actuators have also been used in the development of MR-compatible surgical robots. Pneumatic actuators offer several advantages over USM and hydraulic systems. As these actuators are completely free of electrical circuitry when implemented with optical sensors, they do not introduce artifacts to the MR images. Easily powered by a compressed gas supply, they do not pose a contamination hazard, in contrast to hydraulic systems. The gas dynamics also make pneumatic actuators favorable for fast or force-controlled applications [9].

In light of these desirable characteristics, several MR-compatible devices are reported to employ either double-acting pneumatic piston cylinders or pneumatic stepper motors. Stoianovici et al invented PneuStep, a precision pneumatic stepper motor that has successfully operated within a 7T scanner [10]. Using a 6-DOF MR-guided robot with PneuStep technology, Muntener et al reported a precision of 2.02 mm for prostatic needle placement in vivo in canines [11].

A frequently cited choice of pneumatic piston cylinder is the MR-compatible model line manufactured by Airpot Corp (Norwalk, CT). With these actuators Song et al achieved an average position accuracy of 0.3 mm by incorporating external damping into their 4-DOF robot for prostate brachytherapy (in 3T scanner) [12]. Another system for prostatic interventions was developed by Fischer et al and demonstrated a very low impact on SNR of 5% [13]. Pneumatic piston cylinders have also been employed in MR-guided robots for abdominal and breast interventions [14],[15].

The dynamics for pneumatic piston-cylinder actuators are highly nonlinear but precision control with them has been demonstrated in both surgical and non-surgical applications [13-16]. Richer and Hurmuzlu introduced a detailed mathematical model for the dynamics of these actuators and they proceeded to achieve precision force tracking using sliding mode control (SMC) [17],[18]. Yang et al reported 1 mm needle tip accuracy for a 1-DOF MR-compatible device using a fiber-optic 3D force sensor [15]. Zhu and Barth achieved 0.05 mm accuracy using a composite adaptive-SMC force tracker for an industrial robot [16]. While accuracy on the order of nanometers has been shown for industrial actuators, it has yet to be achieved with MR-compatible cylinders.

In this paper we report 0.018 mm accuracy for a 1-DOF MR-compatible pneumatic actuator. To realize these results it was crucial to use a detailed model of mass flow dynamics from the literature. We did not include any force sensor but measured only position and pressures. Compared to prior work with pneumatic medical robots, our use of fewer sensors resulted in a simpler, less expensive system with better position accuracy.

SYSTEM MODELING

Modeling the dynamics of pneumatic piston-cylinder actuators has been well-defined and verified in the literature. A typical model includes the dynamics of the piston-load interaction, the cylinder chamber dynamics and the mass flow through the control valve. Figure 1 provides an illustration of the actuator considered.

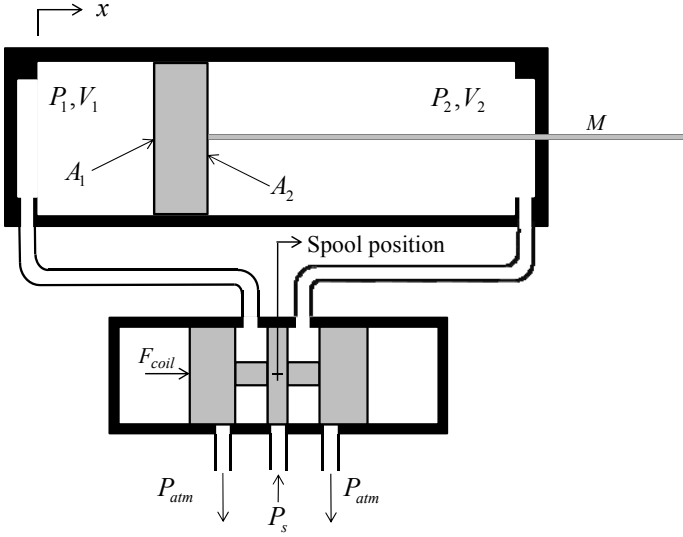


FIGURE 1. PISTON-CYLINDER & SPOOL CONTROL VALVE

Piston-Load Dynamics

In medical applications, the reaction force exerted by tissue on a needle is generally unpredictable, as tissue properties vary by patient and procedure. Inclusion of this force in the piston-load dynamics would require the development of a special MR-compatible fiber optic force sensor. A simpler approach was taken by neglecting this force and relying on the robustness of the sliding mode controller to compensate for this error. Thus the equation of motion for a double-acting piston cylinder is

$$M \ddot{x} = P_1 A_1 - P_2 A_2 - P_{atm} A_r - \beta \dot{x} \quad (1)$$

In Eq. (1) the area of the piston rod is calculated $A_r = A_1 - A_2$. Equation (1) includes a viscous frictional interaction between piston and chamber wall. The mass M is the combined moving mass of the piston, piston rod and needle.

Chamber Dynamics

The relationship between the piston-load dynamics and chamber dynamics is evident from the first time derivative of Eq. 1,

$$M \ddot{x} = \dot{P}_1 A_1 - \dot{P}_2 A_2 - \beta \ddot{x} \quad (2)$$

Because robots for medical interventions typically operate at a low bandwidth, isothermal conditions for the gas dynamics

were assumed. Thus, from [17] the first time derivative of the chamber pressures $\dot{P}_i, i = 1, 2$ is

$$\dot{P}_i = \frac{RT}{V_i} \dot{m}_i - \frac{P_i \dot{V}_i}{V_i} \quad (3)$$

In Eq. 3, R is the specific ideal gas constant and T is the ambient temperature. The mass flow \dot{m}_i into the i th chamber is the focus of our controller design. Thus we turn our attention to the dynamic model of the mass flow proportional valve.

Valve Mass Flow Dynamics

In our system a mass flow proportional valve is used, the dynamics of which have been well-defined by Richer and Hurmuzlu [17]. Based on work by Ben-Dov and Salcudean, the mass flow \dot{m}_1 into chamber 1 is defined as [19]

$$\dot{m}_1 = A_v \Psi_1(P_u, P_d) \quad (4)$$

In Eq. 4 the area normalized mass flow through an orifice $\Psi_1(P_u, P_d)$ is dependent on P_u and P_d , the pressures upstream and downstream of the orifice. This function is given by

$$\Psi(P_u, P_d) = \begin{cases} \frac{C_1 C_f P_u}{\sqrt{T}} & \text{if } \frac{P_d}{P_u} \leq C_r \text{ (choked)} \\ \frac{C_2 C_f P_u}{\sqrt{T}} \left(\frac{P_d}{P_u}\right)^{1/k} \sqrt{1 - \left(\frac{P_d}{P_u}\right)^{(k-1)/k}} & \text{otherwise (unchoked)} \end{cases} \quad (5)$$

In Eq. 5, $k = c_p/c_v$ is the ratio of specific heats, C_f is a dimensionless discharge coefficient dependent on orifice geometry, and C_r is the pressure ratio that determines whether the flow is choked or unchoked. For air, $C_r = 0.5286$. The constants are given by

$$C_r = \left(\frac{2}{k+1}\right)^{\frac{k}{k-1}} \quad (6)$$

$$C_1 = \sqrt{\frac{k}{R} \left(\frac{2}{k+1}\right)^{(k+1)/(k-1)}} \quad \text{and} \quad C_2 = \sqrt{\frac{2k}{R(k-1)}} \quad (7)$$

In Eq. 7, R is the specific ideal gas constant.

The upstream and downstream pressures for \dot{m}_1 are determined by

$$\Psi_1(P_u, P_d) = \begin{cases} \Psi(P_s, P_1) & \text{for } A_v \geq 0 \\ \Psi(P_1, P_{atm}) & \text{for } A_v < 0 \end{cases} \quad (8)$$

Thus, we define A_v to be positive when chamber 1 is charging and negative when chamber 1 is exhausting.

By expressing the mass flow as area normalized mass flow, Zhu and Barth showed explicitly how a single valve command A_v determines the mass flow to both chambers [16]. The mass flow \dot{m}_2 into chamber 2 is thus given by

$$\dot{m}_2 = -A_v \Psi_2(P_u, P_d) \quad (9)$$

By our definition of the sign of A_v , for A_v positive, chamber 2 is exhausting, and for A_v negative, chamber 2 is charging. Thus, the area normalized mass flow for chamber 2 is given by

$$\Psi_2(P_u, P_d) = \begin{cases} \Psi(P_2, P_{atm}) & \text{for } A_v \geq 0 \\ \Psi(P_s, P_2) & \text{for } A_v < 0 \end{cases} \quad (10)$$

Richer and Hurmuzlu provide a model for calculating A_v from spool position [17]. We used this model to correlate A_v to the valve voltage command. This modeling and Eqs. 4 to 10 provide the complete dynamics for the valve mass flow.

SLIDING MODE CONTROLLER

The robustness of sliding mode control lends itself well to applications involving unmodeled dynamics. Because it was undesirable to measure the reactive force of the tissue on the needle, an SMC was chosen in order to overcome inaccuracy due to this tissue force. Slotine and Li present a commonly used time-varying sliding surface s for an n th-order system as [20]

$$s = \left(\frac{d}{dt} + \lambda \right)^{n-1} e \quad (11)$$

The system of Eq. 2 is 3rd-order. However, it was necessary to act on the integral of the error e to achieve the desired accuracy of steady state positioning. Thus, the sliding surface took the form

$$s = \left(\frac{d}{dt} + \lambda \right)^3 \int e \quad (12)$$

By conventional SMC theory we define the error $e = x - x_d$. The result of expanding Eq. 12 is

$$s = \ddot{e} + 3\lambda\dot{e} + 3\lambda^2e + \lambda^3 \int e \quad (13)$$

Then the sliding mode equation is obtained by taking the time derivative of s and substituting Eq. 2 into \dot{s} :

$$\dot{s} = \frac{1}{M} (\dot{P}_1 A_1 - \dot{P}_2 A_2 - \beta \dot{x}) - \ddot{x}_d + 3\lambda\dot{e} + 3\lambda^2e + \lambda^3e \quad (14)$$

Our choice of control law A_v must ensure that the “distance” s^2 to the sliding surface decreases along all system trajectories. That is, we want s^2 to be a Lyapunov-like function of the closed-loop system. Mathematically this requirement is given by

$$\frac{1}{2} \frac{d}{dt} s^2 \leq -\eta |s| \quad (15)$$

The robustness constant η is strictly positive.

Using the chain law for differentiation, Eq. 15 yields $\dot{s} \leq -\eta \text{sgn}(s)$, where $\text{sgn}(s) = |s|/s$. Substitution of this result and Eq. 3 into Eq. 14 yields the control law

$$A_v = \frac{\ddot{x}_d - f(P_i, V_i, \dot{V}_i, \ddot{x}) - 3\lambda\dot{e} - 3\lambda^2e - \lambda^3e - \eta \text{sgn}(s)}{g(V_i, \Psi_i)} \quad (16)$$

The functions f and g are given by

$$f(P_i, V_i, \dot{V}_i, \ddot{x}) = \frac{1}{M} \left(-\frac{P_1 A_1}{V_1} \dot{V}_1 + \frac{P_2 A_2}{V_2} \dot{V}_2 - \beta \ddot{x} \right) \quad (17)$$

$$g(V_i, \Psi_i) = \frac{RT}{M} \left(\frac{A_1}{V_1} \Psi_1 + \frac{A_2}{V_2} \Psi_2 \right) \quad (18)$$

Using Eqs. 16-18 and the model of the valve mass flow dynamics, we designed a sliding mode controller.

EXPERIMENTAL SETUP

The experimental setup is shown in Fig. 2. The Airpel piston-cylinder (Airpot Corp., CT) is known from the literature to be MR-compatible. The stroke length and maximum needle insertion depth is 79.1 mm. All pneumatic fittings on the actuator are comprised of brass (Beswick Eng. Co., NH). A diamond-point 13-gauge needle and linear potentiometer (Midori, Japan) are coupled to the piston rod. The phantom material is polyvinyl chloride (PVC) with a liquid plasticizer (M-F Manufacturing, TX). This soft elastic phantom is of the same material as those described by DiMaio and Salcudean, who reported Young’s Moduli in the range of 10 to 100 kPa [21]. The supply pressure and two chamber pressures are measured using three pressure transducers (Festo SDE-16-10V, Germany). The mass flow proportional valve is a 5-way spool valve (Festo MPYE-5-M5-010-B).

We implemented the sliding mode controller using MATLAB Simulink and Real Time Workshop. The supply pressure was in the range of 155 to 160 kPa absolute (7.8 to 8.5 psig). At such a low pressure, special care had to be taken to

precisely calibrate the pressure transducers so as to provide precise calculations of mass flow. Table 2 provides a summary of parameter values for our system.

EXPERIMENTAL RESULTS

Our sliding mode controller successfully tracks desired position inputs of step waveforms. Figure 3 depicts reference and actual positions vs. time that would be well applicable to stereotactic procedures. Needle placement was commanded for five progressively deeper insertions, followed by one retraction. At 28.0 seconds, the final reference step is 1.0 mm before reaching the ultimate target needle insertion depth of 76.0 mm. The corresponding position errors are depicted in Fig. 4. For a total of 12 step commands for the sequence run twice, the mean steady-state position error was 0.018 mm, the maximum steady-state position error was 0.028 mm, and the maximum overshoot was 0.371 mm. The supply and chamber pressures during this experiment are shown in Fig. 5.

TABLE 1. SYSTEM PARAMETER VALUES

A_1	67.9291 mm ²
A_2	60.0864 mm ²
C_f	0.2939
C_r	0.5826
β	5 N/(m/s)
η	2 m/s ³
λ	20 Hz
M	38.6 g
Stroke length	79.1 mm

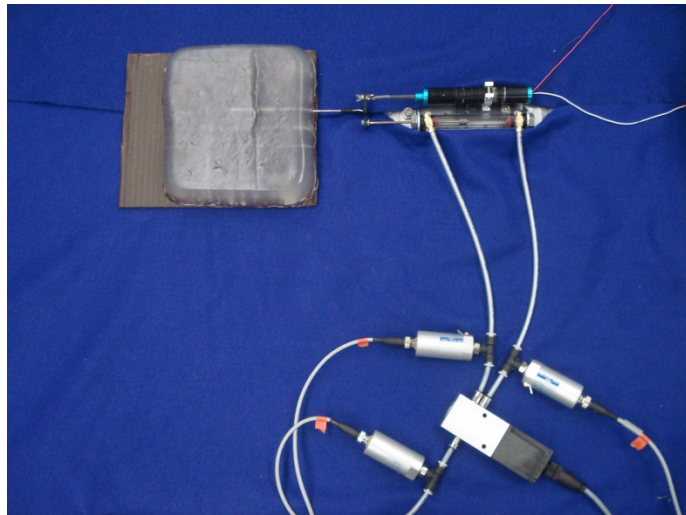


FIGURE 2. PNEUMATIC PISTON-CYLINDER SYSTEM

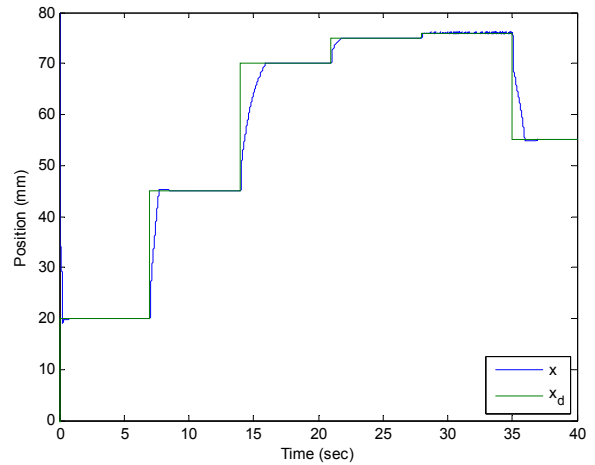


FIGURE 3. POSITION TRACKING

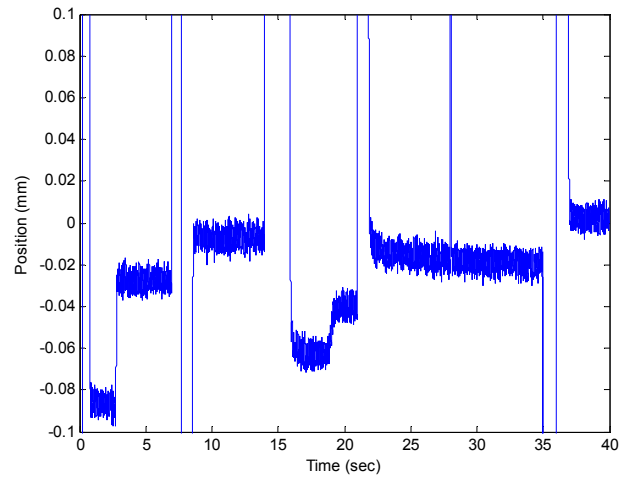


FIGURE 4. POSITION ERROR

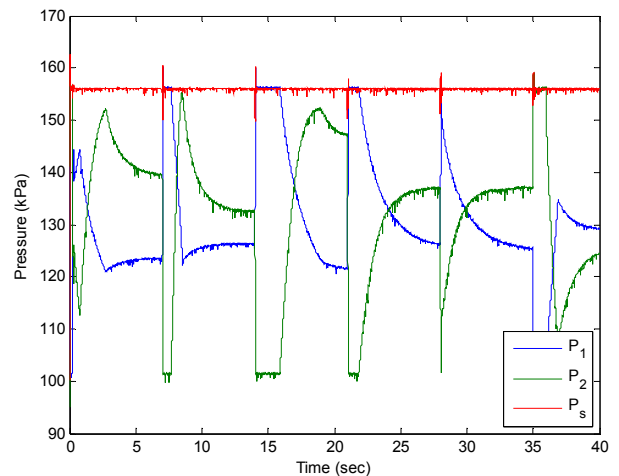


FIGURE 5. SYSTEM PRESSURES

CONCLUSION

Pneumatic piston-cylinder actuators are an ideal choice for MR-compatible surgical robots, as they do not rely on electrical circuitry and they pose no risk of contamination. However, the nonlinearity of the compressed gas dynamics requires a robust controller like sliding mode. Beginning with a known model for the mass flow and chamber dynamics, we developed a sliding mode equation and control law based solely on actuator position. In experimental testing we achieved a mean accuracy of 0.018 mm, and a maximum steady-state error of 0.028 mm. To the authors' knowledge, this is the best accuracy for an MR-compatible pneumatic piston-cylinder system. Additionally, because our system does not rely on a force sensor, we expect it will be easier to implement in the MRI environment.

To pursue the use of this precision controlled pneumatic system for use inside an MRI machine, several modifications must first be made. The linear potentiometer needs to be replaced by an MR-compatible fiber optic encoder, which is commercially available. Given that the valves are not MRI compatible, the plastic pneumatic lines must be extended to about 10 meters total length, with a time-delay compensator added to the controller. Finally, the 1-DOF proof-of-concept system discussed here must be integrated into a multiple DOF surgical robot. Based on the results we report in this paper, these steps will be pursued as future work.

REFERENCES

- [1] Krieger, A., Susil, R., Menard, C., Coleman, J., Fichtinger, G., Atalar, E., and Whitcomb, L., 2005, "Design of a Novel MRI Compatible Manipulator for Image Guided Prostate Interventions," *IEEE Trans. Bio-Med. Eng.*, **52**(2), pp. 306-313.
- [2] Krieger, A., Iordachita, I., Song, S., Cho, N., Guion, P., Fichtinger, G., and Whitcomb, L., 2010, "Development and Preliminary Evaluation of an Actuated MRI-Compatible Robotic Device for MRI-Guided Prostate Intervention," *IEEE ICRA*, Anchorage, AK, pp. 1066-1073.
- [3] Kim, D., Kobayashi, E., Dohi, T., and Sakuma, I., 2002, "A New, Compact MR-Compatible Surgical Manipulator for Minimally Invasive Liver Surgery," *Medical Image Computing and Computer Assisted Intervention*, **2488**, pp. 99-106.
- [4] Moser, R., Gassert, R., Burdet, E., Sacher, L., Woodtli, H.R., Maeder, W., and Bleuler H., 2003, "An MR Compatible Robot Technology," *IEEE ICRA*, Taipei, Taiwan, pp. 670-675.
- [5] Elhawary, H., Zivanovic, A., Davies, B., and Lampérth, M., 2006, "A Review of Magnetic Resonance Imaging Compatible Manipulators in Surgery," *Proc IMechE, Part H: J. of Engineering in Medicine*, **220**(3), pp. 413-424.
- [6] Tsekos, N., Khanicheh, A., Christoforou, E., and Mavroidis, C., 2007, "Magnetic Resonance-Compatible Robotic and Mechatronic Systems for Image-Guided Interventions and Rehabilitation: A Review Study," *Annu. Rev. Biomed. Eng.*, **9**, pp. 351-387.
- [7] Larson, B., Erdman, A., Tsekos, N., Yacoub, E., Tsekos, P., and Koutlas, I., 2004, "Design of an MRI-Compatible Robotic Stereotactic Device for Minimally Invasive Interventions in the Breast," *J. Biomech. Eng.*, **126**(4), pp. 458-465.
- [8] Wang, Y., Cole, G., Su, H., Pilitsis, J., and Fischer, G., 2009, "MRI Compatibility Evaluation of a Piezoelectric Actuator System for a Neural Interventional Robot," *IEEE EMBC*, Minneapolis, MN, pp. 6072-6075.
- [9] Yu, N., Hollnagel, C., Blickenstorfer, A., Kollias, S., and Riener, R., 2008, "Comparison of MRI-Compatible Mechatronic Systems with Hydrodynamic and Pneumatic Actuation," *IEEE/ASME Trans. Mechatronics*, **13**(3), pp. 268-277.
- [10] Stoianovici, D., Patriciu, A., Petrisor, D., Mazilu, D., and Kavoussi, L., 2007, "A New Type of Motor: Pneumatic Step Motor," *IEEE/ASME Trans. Mechatronics*, **12**(1), pp. 98-106.
- [11] Muntener, M., Patriciu, A., Petrisor, D., Schar, M., Ursu, D., Song, D., and Stoianovici, D., 2008, "Transperineal Prostate Intervention: Robot for Fully Automated MR Imaging—System Description and Proof of Principle in a Canine Model," *J. Radiology*, **247**(2), pp. 543-549.
- [12] Song, S., Cho, N., Tokuda, J., Hata, N., Tempany, C., Fichtinger, G., and Iordachita, I., 2010, "Preliminary Evaluation of a MRI-compatible Modular Robotic System for MRI-guided Prostate Interventions," *IEEE RAS & EMBS*, Tokyo, Japan, pp. 796-801.
- [13] Fischer, G., Iordachita, I., Csoma, C., Tokuda, J., DiMaio, S., Tempany, C., Hata, N., and Fichtinger, G., 2008, "MRI-Compatible Pneumatic Robot for Transperineal Prostate Needle Placement," *IEEE/ASME Trans. Mechatronics*, **13**(3), pp. 295-305.
- [14] Zemitte, N., Bricault, I., Fouard, C., Sanchez, B., and Cinquin, P., 2008 "LPR: A CT and MR-Compatible Puncture Robot to Enhance Accuracy and Safety of Image-Guided Interventions," *IEEE/ASME Trans. Mechatronics*, **13**(3), pp. 306-315.
- [15] Yang, B., Tan, U-X., McMillan, A., Gullapalli, R., and Desai, J., 2010, "Design and Control of a 1-DOF MRI-Compatible Pneumatically Actuated Robot with Long Transmission Lines," *IEEE/ASME Trans. Mechatronics*.
- [16] Zhu, Y., and Barth, E., 2009, "Accurate Sub-Millimeter Servo-Pneumatic Tracking using Model Reference Adaptive Control (MRAC)," *International Journal of Fluid Power*, **1**, pp. 49-57.
- [17] Richer, E., and Hurmuzlu, Y., 2000, "A High Performance Pneumatic Force Actuator System: Part 1—Nonlinear

Mathematical Model,” *ASME J. Dyn. Syst., Meas. Control*, **122**(3), pp. 416-425.

- [18] Richer, E., and Hurmuzlu, Y., 2000, “A High Performance Pneumatic Force Actuator System: Part 2—Nonlinear Controller Design,” *ASME J. Dyn. Syst., Meas. Control*, **122**(3), pp. 426-434.
- [19] Ben-Dov, D., and Salcudean, S., 1995, “A Force-Controlled Pneumatic Actuator,” *IEEE Trans. Robotics & Automation*, **11**(6), pp. 906-911.
- [20] Slotine, J.-J., and Li, W., 1991, *Applied Nonlinear Control*, Prentice Hall, Englewood Cliffs, New Jersey, Chap. 7, pp. 278.
- [21] DiMaio, S., and Salcudean, S., 2003, “Needle Insertion Modeling and Simulation,” *IEEE Trans. Robotics & Automation*, **19**(5), pp. 864-875.